optica

Low-loss, centimeter-scale plasmonic metasurface for ultrafast optoelectronics

Andrew J. Traverso,[1,†] Jiani Huang,[1,†] Thibault Peyronel,[2] Guoce Yang,[3] Tobias G. Tiecke,[2] and Maiken H. Mikkelsen[3,*]

[1]Department of Physics, Duke University, Durham, North Carolina 27708, USA
[2]Facebook Inc., Connectivity Lab, 1 Hacker Way, Menlo Park, California 94025, USA
[3]Department of Electrical and Computer Engineering, Duke University, Durham, North Carolina 27708, USA
*Corresponding author: m.mikkelsen@duke.edu

Received 22 June 2020; revised 5 December 2020; accepted 22 December 2020 (Doc. ID 400731); published 11 February 2021

Plasmonics can dramatically improve the radiative properties of fluorescent materials by precisely tailoring the local density of states, but has largely been dismissed for practical optoelectronic applications due to losses and lack of scalability to macroscopic areas. Here, we demonstrate a low-loss plasmonic metasurface that can collect fast-modulated light with a 3 dB bandwidth exceeding 14 GHz and a 120° acceptance angle and convert it to a directional source with, to the best of our knowledge, a record-high overall efficiency of ∼30%. This large-area metasurface composed of fluorescent dye coupled to nanopatch antennas, exhibits a 910-fold increase in the overall fluorescence and a 133-fold emission rate enhancement—values previously only observable for isolated, highly optimized single nanostructures. Critical for future applications ranging from optoelectronics to biosensing, this metasurface was created over macroscopic areas with scalable techniques and the performance was validated over centimeter-scale regions. In particular, we believe this approach shows promise for the burgeoning field of visible/near-infrared wireless communications, where radical new designs and materials are needed for ultrafast, efficient, omnidirectional detectors and incoherent sources.

https://doi.org/10.1364/OPTICA.400731

1. INTRODUCTION

The optical properties of emitters are closely related to the local electromagnetic environment, which can be strongly modified by plasmonic structures that enable optical fields to be concentrated to deep-subwavelength regions. In this way, plasmonic nanocavities have been widely used to enhance fluorescence [1–6], Raman scattering [7–9], and absorption [10–13], as well as both the rate [1–3,14–16] and directionality of emission [16–19]. Notably, fluorescence enhancements up to 1,340-fold have been observed from single molecules coupled to individual gold bowtie antennas [3]; and emission rate enhancements up to 1,000-fold have been demonstrated for semiconductor quantum dots embedded in film-coupled nanocubes [2]. However, these proof-of-concept demonstrations have been limited to rare occurrences of exceptionally well-coupled emitters to tiny hot spots. Fluorescence enhancements from larger, millimeter-sized areas have been explored using nanoantenna-dot arrays, but relied on fluorescent dyes with an intrinsically very low quantum efficiency (QE) that is unsuitable for practical applications that require a large overall photon conversion efficiency. Crucially, given the inherent losses of plasmonic systems [20], there have been no demonstrations extending these structures to macroscales while achieving a high photon conversion efficiency.

If the core radiative properties of luminescent materials, including lifetime, efficiency, and radiation pattern, could be enhanced over macroscopic areas, it would enable use in a variety of fields from sensing and optoelectronics to free-space optical communications (FSOC). For example, a high-bandwidth incoherent light source could be integrated in the lighting infrastructure to act as a transmitter to achieve visible light communications (VLC) and offer high data throughput densities [21]. A luminescent material with high efficiency and ultrafast response times modulated by a high bandwidth laser would constitute such an incoherent light source [22–24]. On the receiver end, an ideal detector for FSOC would have a large active area, a fast response time, and high fidelity to fully support the highest data rates made possible by an optical frequency standard. In addition, it should be highly efficient to keep transmission intensities low and have a wide detection angle to minimize the pointing and tracking complexity [25]. The commonly used semiconductor photodetectors typically see their response times slow down as their active areas increase, due to junction capacitance, carrier transit, and diffusion times. While this can be compensated for with refractive optics, it ultimately limits the field of view due to the conservation of etendue. Fluorescent dyes can decrease the optical etendue of light collected over a large area with a large field of view and concentrate it onto a small photodiode [26]. However, the intermediate scattering introduces high losses and the decay rate sets a lower limit to the response time of

these luminescent detectors. With fluorescence lifetimes in excess of ~1 ns for known high quantum yield dye in the visible and IR spectrum, luminescent detectors are not fast enough to accommodate high-throughput wireless communications. Plasmonic enhancement offers unprecedented control of the radiative lifetime and radiation pattern of luminescent dyes. However, for practical FSOC and most other optoelectronic applications, this enhancement must be scaled to macroscopic areas while maintaining a high photon conversion efficiency.

Here, we demonstrate a robust and uniform plasmonic enhancement of luminescent dye over centimeter-scale areas with what we believe is both a record-setting high photon conversion efficiency of 28.6% and an ultrafast emission lifetime of ~12 ps corresponding to 133× enhancement in the spontaneous emission rate. The rate enhancement originates from a plasmonic nanocavity structure with a small mode volume. This creates strongly enhanced localized electromagnetic fields in the vicinity of the dye, which increase the transition rate (also referred to as the Purcell effect). Additionally, this dye-coupled plasmonic metasurface absorbs light from wide incidence angles and efficiently generates directional emission with an ultrafast response time that can be modulated at speeds exceeding 14 GHz at a 3 dB level. The structure consists of colloidally synthesized 60 nm, silver nanocubes on a ~7 nm polymer layer with embedded fluorescent dye and an underlying silver film, as shown in Fig. 1(a). This creates a nanogap plasmonic structure with large electric field enhancements up to 80-fold between the silver nanocubes and silver film (see Supplement 1, Fig. S3). To increase the photon conversion efficiency, four separate layers of a photostable high quantum yield (QY) fluorescent dye, Atto 532 (90% QE), are embedded between polymer layers in the gap between the silver film and nanocubes (see Supplement 1 for fabrication details). To maximize the absorption at the plasmon resonance, the nanocubes cover 17% of the surface corresponding to an average spacing of 194 nm between the cubes for a 1.2 cm diameter area, as shown in Fig. 1(b). This results in a ~90% absorption centered at 542 nm, as seen in the reflectance spectrum in Fig. 1(c). The density of nanocubes, which is chosen to maximize the absorption cross section [11] while coupling between adjacent nanocubes, is unlikely because significant coupling has been found to only occur for spacings of ~30 nm or less [27]. For an optimized overall photon conversion efficiency, the dimensions of the structure are chosen to overlap well with both the absorption and emission spectra of the dye to leverage a combination of plasmonic absorption and emission enhancement.

2. CHARACTERIZATION OF FLUORESCENCE ANGULAR DEPENDENCE AND EFFICIENCY

To probe the fluorescence enhancement, a 532 nm continuous wave (cw) laser was focused on the structure to a ~2.2 μm diameter spot and the emission was collected by an imaging spectrograph (see Supplement 1). A 910-fold enhancement in the fluorescence intensity is observed compared to the emission from a control sample on glass with the same dye concentration and layer structure. This is visualized in the inset of Fig. 1(d), where fluorescence from a ~100 μm diameter area is shown for both the plasmonic sample and the control on glass using the same excitation conditions. The plasmonic sample is observed to be

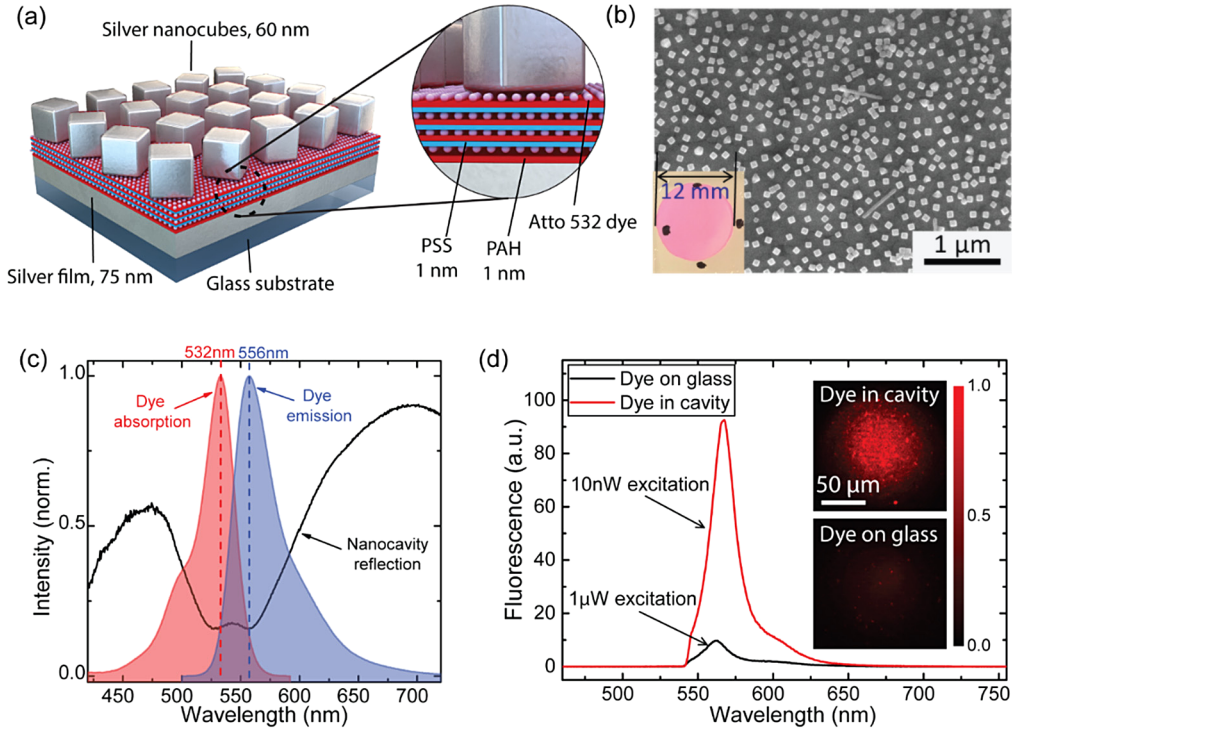

Fig. 1. Sample schematic and characterization. (a) Schematic of the plasmonic structure, which consists of colloidally synthesized silver nanocubes placed over a silver film and separated by a spacer layer consisting of sandwiched dye molecules and polymers. (b) SEM image of the sample. Inset shows an optical microscopy image of the 12 mm sample. (c) Reflectance spectrum of the sample (black), with the plasmon resonance overlapping with both the intrinsic absorption (red shaded region) and emission (blue shaded region) of the fluorescent dye. (d) Fluorescence spectra from the dye on a glass substrate (black) and dye coupled to the plasmonic cavity (red). Different excitation powers are used for the two samples, as labeled in the figure. Inset: 2D fluorescence images for dye on the glass substrate (control) and dye coupled to the plasmonic cavity, under the excitation of a defocused laser beam at 532 nm.

significantly brighter with a uniform fluorescence enhancement over macroscopic areas. In contrast to earlier work [1,2,12,16], the measured enhancement factor of 910-fold is a direct comparison of the fluorescence intensities when the dye is coupled and uncoupled to the plasmonic structure, and is not normalized to the area underneath the nanocubes. The fluorescence intensity exhibited very little deviation over the entire centimeter-scale sample region.

To collect the emission efficiently from a large macroscopic area, the radiation cone of the structure must be narrow. Thus, to determine the radiation pattern of the plasmonic structure, a two-dimensional (2D) k-space image of the sample was taken via a 4f configuration (see Supplement 1). The 532 nm cw laser was focused on the sample plane via a 100×, 0.9 NA objective, and the back focal plane of the objective (i.e., the Fourier plane), is imaged onto an electron multiplying digital camera (Hamamatsu EM-CCD). As shown in Fig. 2(a), the angular dependence of the emission from the sample can be extracted from the 2D k-space image and is normalized to the reflection from a flat silver film. Full-wave simulations [28] of the radiation pattern at the resonant wavelength of 550 nm are also plotted in Fig. 2(a), showing good agreement with the experimental results. From this radiation pattern, the fraction of the emitted light from the sample that is collected by the 100× objective lens is estimated to be ∼84%. Given the ∼1 μm spot size of the laser and an average nanocube spacing of 194 nm, this is estimated to be the collective radiation pattern of ∼27 nanocubes. While previous radiation pattern measurements were performed only on well-isolated individual film-coupled nanocubes [16], these observations demonstrate that emission from a collection of nanocubes does not significantly alter the radiation pattern. This is generally to be expected, because the 194 nm spacing between cubes prevents significant near-field interactions, despite the fact that the measured emission is an aggregate sum of all the excited dye molecules.

From the measurements of the radiation pattern and collection efficiency, the photon-conversion efficiency of the plasmonic structure can be determined using a uniform calibrated light source with a known spectral irradiance. The efficiency is defined as the ratio between the output power from the sample and the laser power incident on the sample (measured after the objective and before hitting the sample). To account for any losses in the experimental setup, the uniform calibrated light source is placed at the sample plane and thus enables the output power directly from the sample to be extracted. Using these measurements in conjunction with our prior observations of the enhanced fluorescence under 10 nW excitation power, the output power collected by the 100× objective lens was determined to be 2.4 nW. Because the collection efficiency of the 0.9 NA objective is estimated to be 84% based on the measured radiation pattern in Fig. 2(a), the total photon conversion efficiency of the plasmonic structure is calculated to be ∼28.6%. To the best of our knowledge, this is the highest efficiency reported for an emitter-coupled plasmonic metasurface, and offers a path forward for the previously reported luminescent detector [26], which was limited by the fluorescent dye's lifetime (1.77 ns) and total efficiency (1.5%).

Next, the performance of the plasmonic structure was characterized for varying incidence angles to determine the angular field of view. The total fluorescent emission intensity was monitored while the angle of the excitation laser was varied relative to the structure. This was accomplished by decoupling the laser from the microscope and varying the incidence angle while the emission was collected by a 5×, 0.15 NA objective lens with a long working distance, and sent to the imaging spectrograph. As can be seen from Fig. 2(a), the fluorescence intensity shows little decrease for incident angles from 0° to 45°, after which it decreases by 50% from normal (0°) to ∼60° incidence. This provides an acceptance angle of at least 120° for significant emission from the sample, which shows potential use as a nearly omnidirectional receiver. Finite-difference time-domain (FDTD) simulations modeling the excitation rate as a function of the incidence angle were also performed that corroborated this behavior, as seen in Fig. 2(a) (see further details in Supplement 1).

Further fluorescence measurements were performed to verify the power dependence of the emission as well as the structure's saturation and damage limits. For FSOC and many other applications, it is imperative that the plasmonic structure provides excellent signal fidelity where the emission not only maintains the modulation rate of the input signal, but also fluctuates linearly relative to the signal. Figure 2(b) shows that the fluorescent emission exhibits a linear dependence on the excitation laser power density below 0.75 W/cm^2. At higher excitation power densities, photobleaching of the dye occurs before saturation of the excited state population can be reached. This measured damage threshold of 0.75 W/cm^2 and the emission intensity at threshold, 0.21 W/cm^2, are well above typical FSOC transmit and receive intensities where low power densities are desirable, which would further improve the long-term photostability of the metasurface. Furthermore, given the rapid expansion of available emitters with new technologies such as organic LEDs [29,30], this approach is

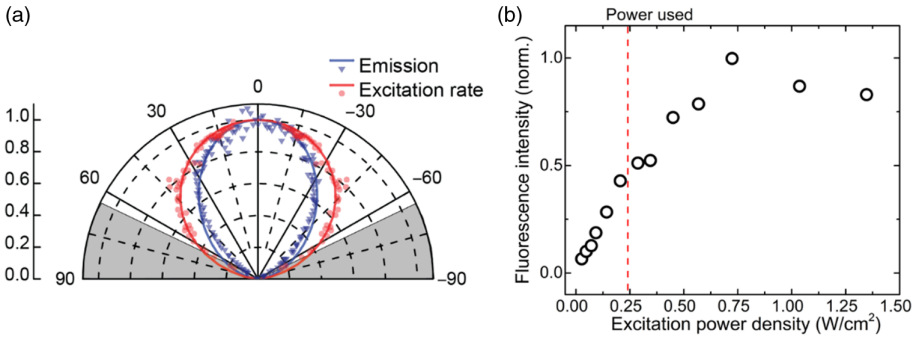

Fig. 2. Emission and excitation behavior. (a) Simulated (lines) and measured (symbols) radiation pattern (blue) and angular dependence of the excitation rate (red) from the plasmonic structure, showing that most emission falls within the numerical aperture of the objective lens (NA = 0.9). The gray-shaded regions represent the angular region that was not collected. (b) The fluorescence intensity as a function of the excitation power when the dye is coupled to the nanocavity, showing a linear region for power densities below 0.75 W/cm^2. The red dashed line indicates the excitation power that is used for the efficiency measurements.

not constrained simply to fluorescent dyes. For ease of demonstration, all measurements for the plasmonic sample were conducted in the linear regime at an excitation power density of 0.24 W/cm^2. For the control sample consisting of dye embedded in the polymer layers on a glass substrate, the dye was found to remain stable up to 13.3 W/cm^2 laser excitation. It should be noted that no photo-blinking was observed in any of the measurements in this work.

3. TIME-RESOLVED MEASUREMENTS OF SPONTANEOUS EMISSION RATE

Next, we investigate the modified spontaneous emission rate experienced by fluorophores coupled to the nanocavity. A strongly enhanced electromagnetic field in the gap region of the cavity causes an increase in the local density of states which, in turn, is directly proportional to the transition rate [31,32]. This is known as the Purcell enhancement, whereby the emission rate can be greatly increased (see Supplement 1). To probe the emission rate of the plasmonic metasurface, time-resolved fluorescence measurements were performed using a 532 nm femtosecond pulsed laser (80 MHz repetition rate, 150 fs pulse length). The emission from the sample was recorded by an avalanche photodiode (APD) connected to a time-correlated single photon counting module. Figure 3(a) shows the normalized temporal dependence of the fluorescence emission from the dye on the glass substrate and the dye coupled to the plasmonic cavity. The control sample of the dye on the glass substrate displays a single exponential decay with a lifetime of 1.6 ns. When the dye molecules are coupled to the plasmonic nanostructure, a significant decrease in the fluorescence lifetime is observed with a decay close to the instrument response function (IRF) of the detector (~30 ps full width at half-maximum). The IRF was obtained by coupling the laser pulse to the APD because its lifetime (150 fs) is over two orders of magnitude below the APD's response time. The data is fit to a single exponential function deconvolved with the IRF revealing a fast decay time of 12 ps for dye coupled to the plasmonic structure. This corresponds to a 133× enhancement in the spontaneous emission rate; however, this only represents a lower bound for the emission rate due to the limited detector resolution. Estimates based on the cavity geometry place the theoretical rate enhancement closer to 1,000-fold (see Supplement 1), which also conforms to prior studies of individual nanocavities [16]. For plasmonic nanocavities in particular, it is also important to consider modifications of the nonradiative processes [33] and the resulting quantum efficiency. The 28.6% conversion efficiency measured from the entire metasurface contains other significant loss mechanisms beyond the nonradiative losses of the nanocavity; however, it provides a lower bound on the quantum efficiency. Also, it should be noted that the decrease in the decay time of the plasmonic sample in Fig. 3(a) is accompanied by a simultaneous increase in the time-integrated fluorescence intensity, as seen in Fig. 1(d). Based on the observed fluorescence enhancement and simulations, the radiative quantum efficiency is estimated to be ~50%. Furthermore, a recent study using a similar plasmonic architecture demonstrated experimental fluorescence decay times in the tens to hundreds of femtoseconds (i.e., an emission rate in the terahertz regime) [34]. This demonstration highlights the potential for future performance gains through this architecture.

While the 12 ps lifetime shown in Fig. 3(a) points toward a potential bandwidth of 83 GHz, it does not verify whether the

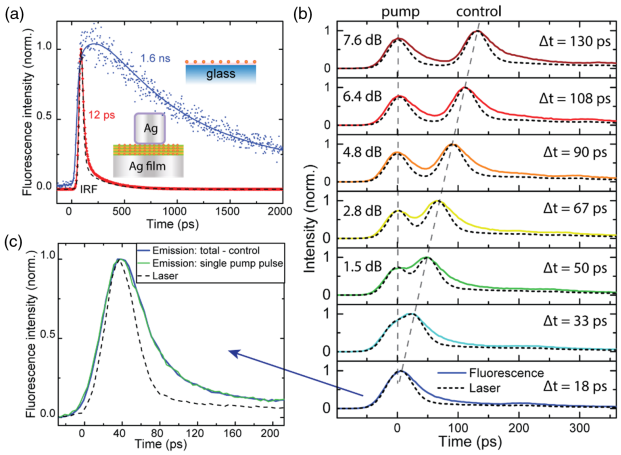

Fig. 3. Lifetime and fast modulation of the plasmonic structure. (a) Normalized time-resolved fluorescence from dye on a glass substrate (blue) and dye coupled to the plasmonic nanocavity (red) along with the IRF shown in black (dashed). Fits to a single exponential function convolved with the IRF are shown in the solid lines. (b) Responses from the plasmonic sample under the excitation of two laser pulses: a pump and a control. The time delay between the pump and the control pulses is controlled by a mechanical delay stage. (c) At a time delay $\Delta t = 18$ ps, the response from the control pulse is subtracted from the response from the two pulses (blue), and is compared to the response from the single pump pulse (green).

emission of the structure can actually be modulated at this rate. For most ultrafast applications, the emission of the structure must be able to follow the modulation of the excitation light with high fidelity. To explore the ultrafast modulation, the 532 nm femtosecond laser was split into two paths: a pump and a control pulse. The control pulse was coupled to a mechanical delay line so that the time delay between the two pulses (that is, the subsequent excitations of the structure) can be controlled. The two pulses are spatially overlapped and focused onto the sample plane via a 20× objective lens, NA of 0.45, with an excitation spot size of ~3 μm (the experimental setup schematic is shown in Fig. S4 of Supplement 1). The resulting response of the plasmonic structure is measured using a fast single-photon APD, as described above. Figure 3(b) displays the response at varying delay times (Δt) between the pump and the control pulses for the emission from both the plasmonic structure (solid curves) and the laser reflection on a flat silver film (dashed curves). It can be seen that the emission from the plasmonic structure closely follows the laser response. For delay times that are larger than 67 ps, the responses from the two pulses are discernible at the 3 dB threshold or above. The distinguishability of the pulses, determined by a comparison of the background level between pulses to the peak height, is given in decibels at each delay time in the figure. The measured response at $\Delta t = 70$ ps suggests a modulation rate exceeding 14 GHz for a distinguishability at the level of 3 dB.

The responses from the two laser pulses is almost indistinguishable when the delay time, Δt, is approaching or is below the detector resolution (~30 ps). In this case, because two pulses are present, deconvolution with the IRF cannot be used to increase the time resolution. To elucidate if the emission from the first pulse modifies the response from the second pulse for delay times below the detector resolution, we subtract the temporal response caused by a single excitation pulse from the temporal response with both pulses present. As seen in Fig. 3, where $\Delta t = 18$ ps, there is very

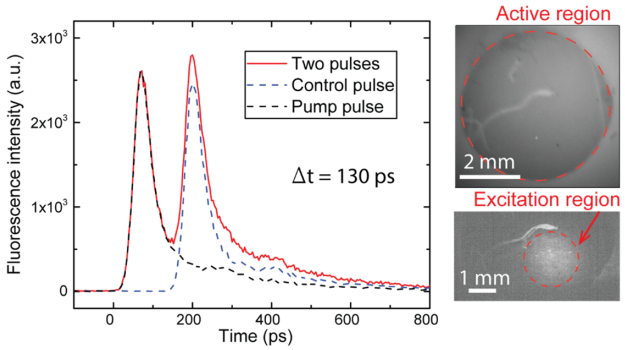

Fig. 4. Fast modulation under a large excitation area. At a time delay $\Delta t = 130$ ps, the responses from each individual pulse, the pump pulse (black dashed) and the control pulse (blue dashed), are shown compared to the response from both pulses (red solid). The region with film-coupled nanocubes (active region) is measured to be 5 mm, while the excitation laser spot is determined to be 2 mm.

good agreement between the remaining emission after subtraction and the emission from a single pulse even when the time delay between the two pulses is below the detector resolution. This shows that the fluorescence emission from the plasmonic sample is not altered or modified by the two excitations. This suggests that, despite the limited detector resolution, the actual 3 dB bandwidth is likely closer to 83 GHz as extracted from lifetime measurements, given that no difference is observed at higher modulation rates between the laser and the emission.

For practical applications, a large effective area is essential for an optical receiver while maintaining a fast response time. The measured directional radiation pattern allows the emission from a large area on the plasmonic sample to be collected. Thus, we extend the fast modulation measurements given above to a millimeter-scale large area. To achieve large area excitation, the objective is replaced by an achromatic lens with a focal length of 200 mm providing a ~2 mm diameter excitation area. Figure 4 shows the responses from two pulses (red solid), the pump pulse (black dashed) and the control pulse (blue dashed), respectively, at a delay time of $\Delta t = 130$ ps. The two pulses are clearly distinguishable. The response from a 2 mm area displays the same behavior as the one measured using a 3 μm laser excitation spot size in Fig. 3(b), at the same delay time. Additionally, the detected photon counts on the APD indicate that the emission from such a large area on the plasmonic sample can be effectively collected, owing to the directional radiation pattern, as measured in Fig. 2(a).

4. CONCLUSION

In conclusion, we have demonstrated that plasmonics can be used to significantly enhance the properties of luminescent materials uniformly over large centimeter-scale regions while maintaining a record-setting high photon conversion efficiency of ~30%. Fluorescent dyes were embedded in a metasurface consisting of plasmonic nanogap cavities resulting in a 910-fold fluorescence enhancement and ultrafast, detector-limited 12 ps emission. Using two 150 fs laser pulses, fast modulation of the fluorescence emission was realized with a 3 dB modulation bandwidth exceeding 14 GHz and likely approaching 80 GHz or greater. The ultrafast response observed from a macroscopic area is indistinguishable from the performance at the micrometer scale, demonstrating no loss of bandwidth (i.e., "smearing") despite that the measured response originates from nanostructures millimeters apart. Additionally, the metasurface absorbs light from wide incidence angles and efficiently generates directional emission with an ultrafast response time, which is critical, for example, for luminescent detectors for FSOC. As a transmitter for visible light communications, the demonstrated structure could provide an alternative to slow LEDs as a fast source of incoherent light. These results establish that a plasmonic metasurface can be tailored to form a large-scale, low-loss and ultrafast luminescent material, paving the way for a profoundly new approach to on-chip design including high-data-rate FSOC as well as effectively providing new material building blocks for ultrafast optoelectronic and sensing components.

Funding. Facebook Inc.; Air Force Office of Scientific Research (FA9550-15-1-0301, FA9550-18-1-0326).

Acknowledgment. Author Maiken H. Mikkelsen acknowledges support from the AFOSR.

Disclosures. The authors declare no conflicts of interest.

Supplemental document. See Supplement 1 for supporting content.

†These authors contributed equally to this paper.

REFERENCES

1. A. Rose, T. B. Hoang, F. McGuire, J. J. Mock, C. Ciracì, D. R. Smith, and M. H. Mikkelsen, "Control of radiative processes using tunable plasmonic nanopatch antennas," Nano Lett. **14**, 4797–4802 (2014).
2. T. B. Hoang, G. M. Akselrod, C. Argyropoulos, J. Huang, D. R. Smith, and M. H. Mikkelsen, "Ultrafast spontaneous emission source using plasmonic nanoantennas," Nat. Commun. **6**, 7788 (2015).
3. A. Kinkhabwala, Z. Yu, S. Fan, Y. Avlasevich, K. Müllen, and W. E. Moerner, "Large single-molecule fluorescence enhancements produced by a bowtie nanoantenna," Nat. Photonics **3**, 654–657 (2009).
4. H. Szmacinski, R. Badugu, F. Mahdavi, S. Blair, and J. R. Lakowicz, "Large fluorescence enhancements of fluorophore ensembles with multilayer plasmonic substrates: comparison of theory and experimental results," J. Phys. Chem. C **116**, 21563 (2012).
5. F. Tam, G. P. Goodrich, B. R. Johnson, and N. J. Halas, "Plasmonic enhancement of molecular fluorescence," Nano Lett. **7**, 496 (2007).
6. W. Zhang, F. Ding, W.-D. Li, Y. Wang, J. Hu, and S. Y. Chou, "Giant and uniform fluorescence enhancement over large areas using plasmonic nanodots in 3D resonant cavity nanoantenna by nanoimprinting," Nanotechnology **23**, 225301 (2012).
7. S.-Y. Ding, J. Yi, J.-F. Li, B. Ren, D.-Y. Wu, R. Panneerselvam, and Z.-Q. Tian, "Nanostructure-based plasmon-enhanced Raman spectroscopy for surface analysis of materials," Nat. Rev. Mater. **1**, 16021 (2016).
8. M. Rycenga, X. Xia, C. H. Moran, F. Zhou, D. Qin, Z. Li, and Y. Xia, "Generation of hot spots with silver nanocubes for single-molecule detection by surface-enhanced Raman scattering," Angew. Chem. (Int. Ed.) **50**, 5473–5477 (2011).
9. M. Yi, D. Zhang, P. Wang, X. Jiao, S. Blair, X. Wen, and Q. Fu, "Plasmonic interaction between silver nano-cubes and a silver ground plane studied by surface-enhanced Raman scattering," Plasmonics **6**, 515–519 (2011).
10. N. I. Landy, S. Sajuyigbe, J. J. Mock, D. R. Smith, and W. J. Padilla, "Perfect metamaterial absorber," Phys. Rev. Lett. **100**, 1–4 (2008).
11. G. M. Akselrod, J. Huang, T. B. Hoang, P. T. Bowen, L. Su, D. R. Smith, and M. H. Mikkelsen, "Large-area metasurface perfect absorbers from visible to near-infrared," Adv. Mater. **27**, 8028–8034 (2015).
12. G. M. Akselrod, T. Ming, C. Argyropoulos, T. B. Hoang, Y. Lin, X. Ling, D. R. Smith, J. Kong, and M. H. Mikkelsen, "Leveraging nanocavity harmonics for control of optical processes in 2D semiconductors," Nano Lett. **15**, 3578–3584 (2015).
13. W. Raja, A. Bozzola, P. Zilio, E. Miele, S. Panaro, H. Wang, A. Toma, A. Alabastri, F. De Angelis, and R. P. Zaccaria, "Broadband absorption enhancement in plasmonic nanoshells-based ultrathin microcrystalline-Si solar cells," Sci. Rep. **6**, 24539 (2016).

14. O. L. Muskens, V. Giannini, J. A. Sánchez-Gil, and J. Gómez Rivas, "Strong enhancement of the radiative decay rate of emitters by single plasmonic nanoantennas," Nano Lett. **7**, 2871–2875 (2007).
15. K. J. Russell, T. Liu, S. Cui, and E. L. Hu, "Large spontaneous emission enhancement in plasmonic nanocavities," Nat. Photonics **6**, 459–462 (2012).
16. G. M. Akselrod, C. Argyropoulos, T. B. Hoang, C. Ciracì, C. Fang, J. Huang, D. R. Smith, and M. H. Mikkelsen, "Probing the mechanisms of large Purcell enhancement in plasmonic nanoantennas," Nat. Photonics **8**, 835–840 (2014).
17. T. Kosako, Y. Kadoya, and H. F. Hofmann, "Directional control of light by a nano-optical Yagi–Uda antenna," Nat. Photonics **4**, 312–315 (2010).
18. H. Aouani, O. Mahboub, E. Devaux, and T. W. Ebbesen, "Plasmonic antennas for directional sorting of fluorescence emission," Nano Lett. **11**, 2400–2406 (2011).
19. H. Aouani, O. Mahboub, N. Bonod, E. Devaux, E. Popov, H. Rigneault, T. W. Ebbesen, and J. Wenger, "Bright unidirectional fluorescence emission of molecules in a nanoaperture with plasmonic corrugations," Nano Lett. **11**, 637–644 (2011).
20. S. V. Boriskina, T. A. Cooper, L. Zeng, G. Ni, J. K. Tong, Y. Tsurimaki, Y. Huang, L. Meroueh, G. Mahan, and G. Chen, "Losses in plasmonics: from mitigating energy dissipation to embracing loss-enabled functionalities," Adv. Opt. Photon. **9**, 775–827 (2017).
21. A. Jovicic, J. Li, and T. Richardson, "Visible light communication: Opportunities, challenges and the path to market," IEEE Commun. Mag. **51**(12), 26–32 (2013).
22. R. Ferreira, E. Xie, J. Mckendry, and S. Rajbhandari, "High bandwidth GaN-based micro-LEDs for multi-Gb/s visible light communications," IEEE Photon. Technol. Lett. **28**, 2023–2026 (2016).
23. M. S. Islim, R. X. Ferreira, X. He, E. Xie, S. Videv, S. Viola, S. Watson, N. Bamiedakis, R. V. Penty, I. H. White, A. E. Kelly, E. Gu, H. Haas, and M. D. Dawson, "Towards 10 Gb/s orthogonal frequency division multiplexing-based visible light communication using a GaN violet micro-LED," Photon. Res. **5**, A35–A43 (2017).
24. Y. Zhou, J. Zhao, M. Zhang, J. Shi, and N. Chi, "2.32 Gbit/s phosphorescent white LED visible light communication aided by two-staged linear software equalizer," in *10th International Symposium on Communication Systems, Networks and Digital Signal Processing (CSNDSP)* (2016), pp. 8–11.
25. J. C. Valencia-Estrada, J. García-Márquez, S. Topsu, and L. Chassagne, "Optical antenna for a visible light communications receiver," Proc. SPIE **10559**, 105590L (2018).
26. T. Peyronel, K. J. Quirk, S. C. Wang, and T. G. Tiecke, "Luminescent detector for free-space optical communication," Optica **3**, 787–792 (2016).
27. M. J. Rozin, D. A. Rosen, T. J. Dill, and A. R. Tao, "Colloidal metasurfaces displaying near-ideal and tunable light absorbance in the infrared," Nat. Commun. **6**, 7325 (2015).
28. J. Yang, J. P. Hugonin, and P. Lalanne, "Near-to-far field transformations for radiative and guided waves," ACS Photon. **3**, 395–402 (2016).
29. S. Reineke, F. Lindner, G. Schwartz, N. Seidler, K. Walzer, B. Lüssem, and K. Leo, "White organic light-emitting diodes with fluorescent tube efficiency," Nature **459**, 234–238 (2009).
30. H. Lee, H. Cho, C.-W. Byun, J.-H. Han, B.-H. Kwon, S. Choi, J. Lee, and N. S. Cho, "Color-tunable organic light-emitting diodes with vertically stacked blue, green, and red colors for lighting and display applications," Opt. Express **26**, 18351–18361 (2018).
31. P. A. M. Dirac, "The quantum theory of the emission and absorption of radiation," Proc. R. Soc. A **114**, 243–265 (1927).
32. M. Sargent, M. O. Scully, and W. E. Lamb, *Laser Physics* (Addison-Wesley, 1974).
33. N. Kongsuwan, A. Demetriadou, R. Chikkaraddy, F. Benz, V. A. Turek, U. F. Keyser, J. J. Baumberg, and O. Hess, "Suppressed quenching and strong-coupling of Purcell-enhanced single-molecule emission in plasmonic nanocavities," ACS Photon. **5**, 186–191 (2018).
34. Y. Zhang, W. Chen, T. Fu, J. Sun, D. Zhang, Y. Li, S. Zhang, and H. Xu, "Simultaneous surface-enhanced resonant Raman and fluorescence spectroscopy of monolayer $MoSe_2$: determination of ultrafast decay rates in nanometer dimension," Nano Lett. **19**, 6284–6291 (2019).